ACS APPLIED MATERIALS & INTERFACES

Research Article

www.acsami.org

Nanocomposites with Graft Copolymer-Templated Mesoporous $MgTiO_3$ Perovskite for CO_2 Capture Applications

Dong Kyu Roh, Sang Jin Kim, Harim Jeon, and Jong Hak Kim*

Department of Chemical and Biomolecular Engineering, Yonsei University, 262 Seongsanno, Seodaemun-gu, Seoul 120-749, South Korea

Supporting Information

ABSTRACT: Mesoporous $MgTiO_3$ perovskite with a high porosity and interfacial properties were synthesized via a solvothermal reaction at 150 °C for 10 h using a graft copolymer, i.e., poly(vinyl chloride)-g-poly(oxyethylene methacrylate) (PVC-g-POEM) with a well-ordered micellar morphology as a structure-directing agent. A PVC-g-POEM graft copolymer with a wormlike morphology was utilized as a soft matrix to prepare a mixed matrix membrane (MMM) with mesoporous $MgTiO_3$ perovskite through a solution-casting method. The structure and morphology of PVC-g-POEM graft copolymer was carefully tuned by controlling polymer-solvent interactions, as characterized by transmission electron microscopy (TEM). The average pore diameter of the $MgTiO_3$ perovskite was 10.4 nm, which is effective in facilitating gas transport via Knudsen diffusion through mesopores as well as improving interfacial contact with the organic polymer matrix. Because of a high porosity (0.56), the density of mesoporous $MgTiO_3$ (1.75 g/cm^3) was much lower than that of dense nonporous $MgTiO_3$ (4 g/cm^3) and not significantly higher than that of PVC-g-POEM (1.25 g/cm^3), leading to a uniform distribution of $MgTiO_3$ in MMM. The permeability of MMM with $MgTiO_3$ was greater than those of MMM with only MgO or TiO_2, indicating the simultaneous improvement of solubility and diffusivity in the former, as supported by CO_2 temperature-programmed desorption (TPD) measurements. The MMM with $MgTiO_3$ 25 wt % exhibited a CO_2 permeability improvement of 140% up to 138.7 Barrer (1 Barrer = 1×10^{-10} cm^3(STP) cm cm^{-2} s^{-1} cmHg^{-1}) without a large loss of CO_2/N_2 selectivity.

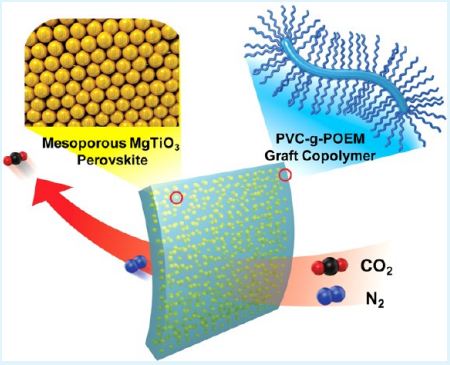

KEYWORDS: *perovskite, mesoporous $MgTiO_3$, graft copolymer, CO_2 permeability, mixed matrix membrane*

INTRODUCTION

Mesoporous metal oxides are of great interest because their morphology and structure play a pivotal role in various applications such as dye-sensitized solar cells, fuel cells, water splitting, lithium batteries and electrochemical capacitors.[1−3] Typically, their pore sizes range between 2 and 50 nm, which is much larger than the size of most gas molecules (e.g., CO_2, 3.3 Å; N, 2.89 Å). Thus, mesoporous materials were limited in membrane-based gas separation, in which micropores are more effective in separating gas mixture.[4−11]

Because polar groups such as ether groups have a strong affinity for CO_2, there have been many studies of gas separation membranes based on poly(ethylene oxide) (PEO).[12−14] However, neat PEO tends to crystallize because of the helical structure of the chains and as a consequence, it possesses a low gas permeability necessitating modification of PEO. The Freeman group prepared highly branched, crosslinked PEO membranes with a high CO_2 solubility and good mechanical stability.[13,14] A block copolymer consisting of two different polymer segments has also been utilized to modify the PEO structure, as reported by the Peinemann group.[15] Ionic liquid-based membranes have also been extensively investigated by the Gin and Noble group as gas separation membranes because of their strong affinity for CO_2.[16,17] Recently, the Lodge group also synthesized triblock copolymer membranes containing an ionic liquid mid-block, which shows a high CO_2 permselectivity.[18]

Conventional polymeric membranes generally suffer from the trade-off between permeability and selectivity, which remains as one of the most important challenges for commercialization.[4] Nanocomposites or mixed matrix membranes (MMMs) are one of the promising classes of membranes in which the properties of both polymer and inorganic phases can be combined to improve the resulting permselectivity, mechanical strength, thermal stability, and processability.[19−23] Typically, MMMs comprise small inorganic nanoparticles such as zeolites, carbon molecular sieves, metal oxides, or carbon nanotubes dispersed in a continuous polymeric matrix. However, most MMMs are based on dense/nonporous or microporous (pore size 0.7−2.0 nm) nanoparticles, which often limit diffusion transport because of the small pore size and low porosity. In addition, transport via the solution mechanism is not fully utilized. The other critical issue in MMMs is the prevention of void formation at the

Received: April 10, 2013
Accepted: June 18, 2013
Published: June 18, 2013

   dx.doi.org/10.1021/am401306p | ACS Appl. Mater. Interfaces 2013, 5, 6615−6621

interface between the inorganic and organic phases, which results in decreased selectivities of gas mixtures.

Here, we present a new class of MMMs based on mesoporous $MgTiO_3$ perovskite templated by a graft copolymer as a structure directing agent. The MMMs demonstrated an improved CO_2 permeability of approximately 140% without a large loss of CO_2/N_2 selectivity compared to the neat polymer matrix. To the best of our knowledge, there have not been any reports on gas separation membranes containing a mesoporous perovskite to date. The structure and morphological properties of the mesoporous $MgTiO_3$ perovskite and the MMM were characterized using transmission electron microscopy (TEM) and scanning electron microscopy (SEM), X-ray diffraction (XRD), N_2 adsorption−desorption measurements, universal tensile machine (UTM) and CO_2 temperature-programmed desorption (TPD). The pure gas permeation properties of CO_2 and N_2 are also reported.

EXPERIMENTAL SECTION

Materials. Magnesium nitrate hexahydrate ($Mg(NO_3)_2{\cdot}6H_2O$), titanium isopropoxide (TTIP), poly(vinyl chloride) (PVC, $M_n \approx 55\,000$ g/mol), poly(oxyethylene methacrylate) (POEM, poly(ethylene glycol) methyl ether methacrylate, $M_n \approx 475$ g/mol), glucose, 1,1,4,7,10,10-hexamethyltriethylene tetramine (HMTETA, 99%), and copper(I) chloride (CuCl, 99%) were purchased from Aldrich. All chemicals were reagent grade and were used as received.

Synthesis of the PVC-g-POEM Graft Copolymer. PVC (6 g) was dissolved in 50 mL of N-methyl pyrrolidone (NMP) by stirring at 90 °C for 4 h. After the solution was cooled to room temperature, 18 g of POEM, 0.1 g of CuCl, and 0.23 mL of HMTETA were added to the solution. The green mixture was stirred until it was homogeneous and was purged with nitrogen for 30 min. The reaction was carried out at 90 °C for 24 h. After polymerization, the resultant mixture was diluted with tetrahydrofuran (THF). After passing the solution through a column containing activated Al_2O_3 to remove the catalyst, the solution was precipitated in methanol. The grafted copolymers were purified by dissolving in THF and reprecipitating into methanol three times. The PVC-*g*-POEM graft copolymer with PVC:POEM = 50:50 (wt %) was obtained in a powder form and dried in a vacuum oven overnight at room temperature.

Synthesis of the Mesoporous $MgTiO_3$ Perovskite. The PVC-g-POEM graft copolymer (0.2 g) with a 50 wt % grafting degree was dissolved in 36 mL of THF, whereas 0.5 g of $Mg(NO_3)_2{\cdot}6H_2O$ and 0.5 g of titanium isopropoxide (TTIP) were dissolved in 4 mL of water. The precursor solution was slowly added drop-wise into the polymer solution under continuous stirring at 500 rpm. After vigorous stirring for 1 h, the solution was transferred to an autoclave and kept at 150 °C for 10 h and then, the autoclave was cooled naturally in air. The precipitate was harvested by centrifugation, followed by washing three times with THF and ethanol. After being dried overnight in an oven at 60 °C, the samples were calcined at 450 °C for 30 min in order to remove the residual organics.

Preparation of the MMMs. Three-tenths of a gram of the PVC-g-POEM graft copolymer was dissolved in 3 mL of THF while the mesoporous $MgTiO_3$ perovskite at different amounts was separately dispersed in THF. The dispersed $MgTiO_3$ perovskite solution was slowly added to the polymer solution. After sufficient mixing using sonication, the PVC-g-POEM/$MgTiO_3$ solution was cast onto Petri dishes. After air drying under ambient conditions for one day, the films were removed from the dishes and placed on Teflon plates. The films were stored under vacuum in an oven at room temperature for 24 h to assist in the removal of the residual THF and then annealed at 50 °C for 24 h. The thicknesses of the membranes were in the range of 60−70 μm.

Permeation Measurements. The pure gas permeation properties were determined using a constant volume/variable pressure apparatus provided by Airrane Co. Ltd. (Korea). The leak rate in the system was measured before starting the permeation experiments and afterward, the pressure increase in the downstream volume was recorded to determine the permeability. The gas permeability was calculated from the steady-state rate of the pressure increase in a fixed downstream volume. The downstream pressure was always less than 20 mmHg, which is very low compared to the upstream pressure (760 mmHg).

Characterization. TEM images were obtained using a JEOL JEM 1010 microscope operating at 300 kV. For the TEM measurements, the graft copolymer was dissolved in a solvent such as THF and then, a drop of this solution was placed onto a standard copper grid. The morphologies of the mesoporous $MgTiO_3$ perovskite and PVC-g-POEM/$MgTiO_3$ perovskite mixed matrix membranes (MMMs) were observed using a field-emission scanning electron microscope (FE-SEM, SUPRA 55VP, Germany, Carl Zeiss). XRD measurements were carried out on a Rigaku RINT2000 wide-angle goniometer with a Cu cathode operated at 40 kV and 300 mA. The specific surface area and pore size diameter were determined from N_2 adsorption−desorption measurements by applying the Brunauer−Emmett−Teller (BET) and Barrett−Joyner−Halenda (BJH) methods. In advance of these measurements, the samples were additionally degassed at 70°C under a dynamic vacuum (1×10^{-2} Torr) for 1 h. Tensile evaluation was performed on a universal testing machine (UTM, a LR10KPlus Series) at a speed of 5 mm/min. To measure the number and strength of basic sites on the mesoporous $MgTiO_3$ perovskite, we conducted CO_2 temperature-programmed desorption (TPD) using BELCAT-M made by Soletek trading Co., Ltd. A 100 mg sample was outgassed at 500 °C for 30 min under flowing He (50 mL/min). The sample surfaces were saturated at 80 °C for 1 h with chemisorbed CO_2 acting as a probe gas by flowing 20% CO_2/He (50 mL/min). The temperature was increased from 25 to 900 °C at a ramping rate of 10 °C/min. The desorbed CO_2 gas from the basic site was detected by a thermal conductivity detector (TCD) under a constant flow rate at 30 mL/min of He carrier gas.

RESULTS AND DISCUSSION

To tune the interfacial properties, we designed an amphiphilic graft copolymer (PVC-g-POEM) consisting of hydrophobic poly(vinyl chloride) (PVC) main chains and hydrophilic poly(oxyethylene methacrylate) (POEM) side chains. The graft copolymer was synthesized via atom transfer radical polymerization (ATRP) using direct initiation of the secondary chlorines of PVC using a previously reported method.[24−26] Graft copolymers are more attractive than block copolymers because of their low cost and ease of synthesis.[27] The PVC-g-POEM graft copolymer was used not only as a matrix in MMMs but also as a structure directing agent for synthesizing mesoporous $MgTiO_3$ perovskite.

The morphology of the PVC-g-POEM graft copolymer was controlled by tuning the interaction strength between the polymer and solvent. Transmission electron microscopy (TEM) images of PVC-g-POEM are shown in Figure 1, where contrast between the PVC and the POEM chains is clear because of the large difference of their electron densities. PVC domains, which have a higher electron density, are dark, whereas the POEM domains are bright. When cast from a tetrahydrofuran (THF) solution, a wormlike, less-ordered, microphase-separated morphology was observed (Figure 1a), which is a typical morphology of graft copolymers.[24,28,29] The solubility parameter (δ) is a good indicator of polymer−solvent interactions. Because the δ of THF closely matches those of PVC and POEM, THF is a good solvent for both chains, where the δ values of THF, PVC, and POEM are 9.6, 9.5, and 10.8 $cal^{1/2}\ cm^{-3/2}$, respectively.[30] The solubility of parameter of POEM was calculated using the group contribution method. In a good solvent, the secondary forces between polymer segments and solvent molecules are strong and thus, both PVC and POEM chains are highly stretched in a spread-out

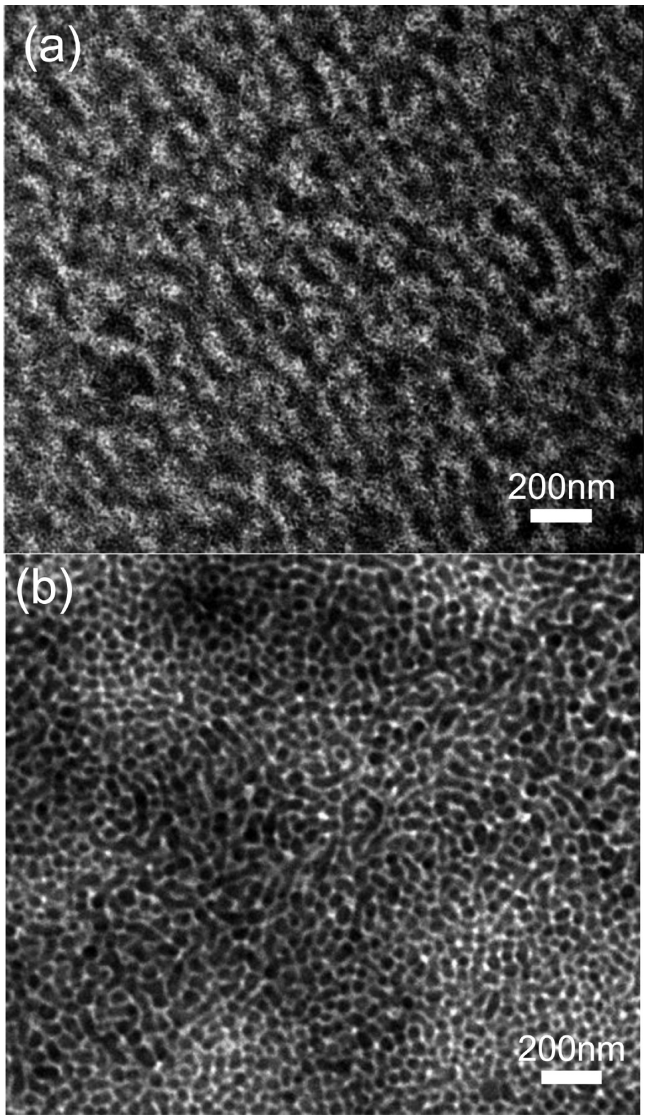

Figure 1. TEM images of PVC-g-POEM graft copolymers cast using (a) THF and (b) a THF/H_2O mixture. The morphologies shown in a and b were used as a matrix to prepare the MMMs and as a template to synthesize mesoporous $MgTiO_3$ perovskite, respectively.

conformation, resulting in a worm-like microphase-separated morphology. When introducing a small amount of H_2O (δ of water = 23.5 $cal^{1/2}$ $cm^{-3/2}$), which is a poor solvent for PVC but a relatively good solvent for POEM, a well-ordered, micellar morphology was observed consisting of a spherical core of PVC chains and continuous corona of POEM chains, as shown in Figure 1b. This is due to the volume contraction of the hydrophobic PVC chains because of the reduced interfacial interaction strength between the polymer and solvent. The average sizes of the isolated PVC core in the micelles were determined to be approximately 70−90 nm.

A PVC-g-POEM graft copolymer with a micellar morphology was applied as a structure directing agent to synthesize mesoporous $MgTiO_3$ perovskite through a solvothermal reaction at 150°C for 10 h utilizing a sol-gel process (Scheme 1). The PVC-g-POEM graft copolymer works well as a structure directing agent due to the flexible, hydrophilic properties of the rubbery POEM chains (glass transition temperature, T_g = −58 °C) and the rigid, hydrophobic properties of glassy PVC chains (T_g = 70 °C).[24−26] Also, the amorphous nature and high molecular weight (weight-average molecular weight, M_w = 1.1 × 10^5 g/mol, polydispersity index, PDI = 2.2) of PVC-g-POEM can generate a large number of mesopores, which facilitates good contact of the organic/inorganic interface and promotes crystallization while maintaining its structural integrity.[31] After calcination at 450 °C, $MgTiO_3$ perovskite with a high porosity, good interconnectivity, and mesopores was generated, as observed in the scanning electron microscopy (SEM) and TEM analysis results shown in images a and b in Figure 2, respectively. The mesoporous $MgTiO_3$ perovskite consisted of small particles aggregated into large clusters of 100−300 nm, which may produce large surface area and facilitate gas transport via Knudsen diffusion through mesopores. The $MgTiO_3$ precursors, magnesium nitrate hexahydrate ($Mg(NO_3)_2{\cdot}6H_2O$) and titanium isopropoxide (TTIP), possess hydrophilic properties and thus are preferentially confined in the hydrophilic POEM chains. Following the in situ formation of crystallites by calcination, the mesopores are generated predominantly from the PVC main chains, which is the core of the micelles.[31]

The XRD pattern (Figure 3a) indicates that the synthesized materials were in a mixture of amorphous and crystalline $MgTiO_3$ perovskite phases.[32] All diffraction peaks could be indexed to the rhombohedral structure, which is consistent with the powder diffraction standards card (No. 06-0494) and previously reported results.[33,34] Furthermore, the presence of an amorphous phase of an inorganic oxide is helpful to improve the interfacial properties with an organic polymer phase. The SEM-energy dispersive spectrometer (EDS) analysis (see Figure S1 in the Supporting Information) shows an almost equimolar composition of Mg and TiO_2, which strongly supports the XRD results. The total pore volume, average pore diameter and surface area of the $MgTiO_3$ perovskite were 0.323 cm^3/g, 10.4 nm and 124.7 g/cm^3, respectively, as determined by N_2 adsorption-desorption measurements (Fig. 3b). This pore size is much larger than the pore size of microporous nanoparticles used in MMMs[19−23] and thus is effective in facilitating gas transport via Knudsen diffusion through mesopores as well as improving interfacial contact with the organic polymer matrix. Furthermore, the pore size of $MgTiO_3$ was much smaller than the coil diameter of PVC-g-POEM graft copolymer (approximately 40 nm) determined from the relation: $R_g = 0.063 \times M_w^{0.5}$, where R_g is the radius of gyration.[35] Thus, the Knudsen diffusion through $MgTiO_3$ mesopores might not be hindered by the pore-filling of graft copolymer.

A PVC-g-POEM graft copolymer with a worm-like morphology was utilized as a soft matrix to prepare a MMM with mesoporous $MgTiO_3$ perovskite through a solution-casting method in THF. The cross-sectional and surface SEM images of the MMM reveal that the mesoporous $MgTiO_3$ perovskite is uniformly distributed throughout the PVC-g-POEM graft copolymer matrix without large aggregation, as shown in Figure 4a and Figure S2 in the Supporting Information. The porosity of mesoporous $MgTiO_3$ perovskite was approximately 0.56, as determined from the relation; porosity = $V_p/(\rho^{-1} + V_p)$, where V_p is the pore volume and ρ is the density of dense nonporous $MgTiO_3$ (4 g/cm^3).[36] Because of a high porosity, the density of mesoporous $MgTiO_3$ (1.75 g/cm^3) is much lower than that of nonporous $MgTiO_3$ and not significantly higher than that of PVC-g-POEM (1.25 g/cm^3), which explains symmetric structure of the MMM with a

dx.doi.org/10.1021/am401306p | ACS Appl. Mater. Interfaces 2013, 5, 6615−6621

Scheme 1. Schematic Illustration for the Synthesis of Mesoporous $MgTiO_3$ Perovskite via a Solvothermal Reaction

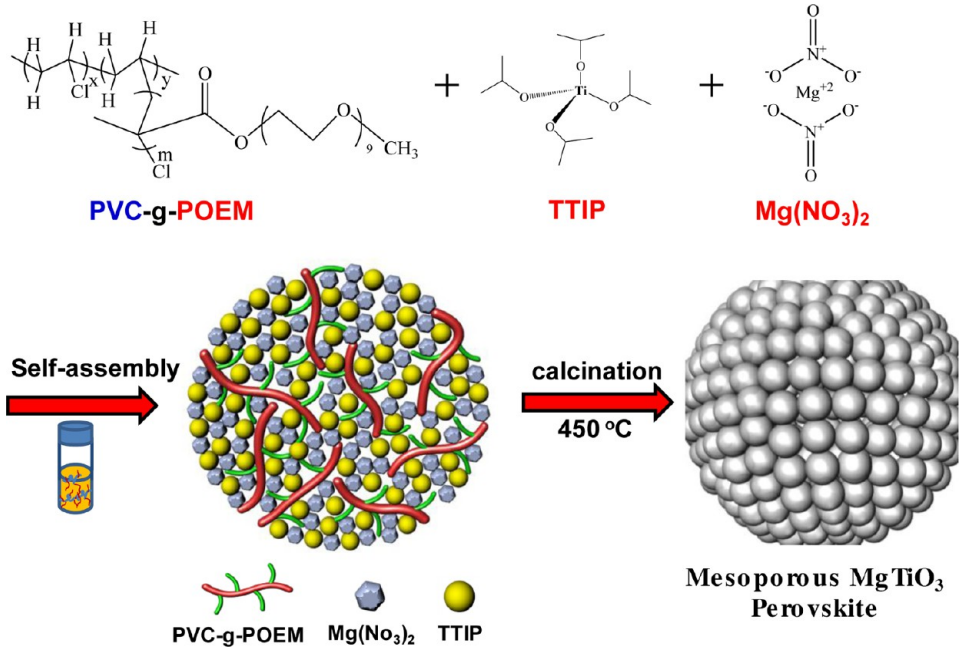

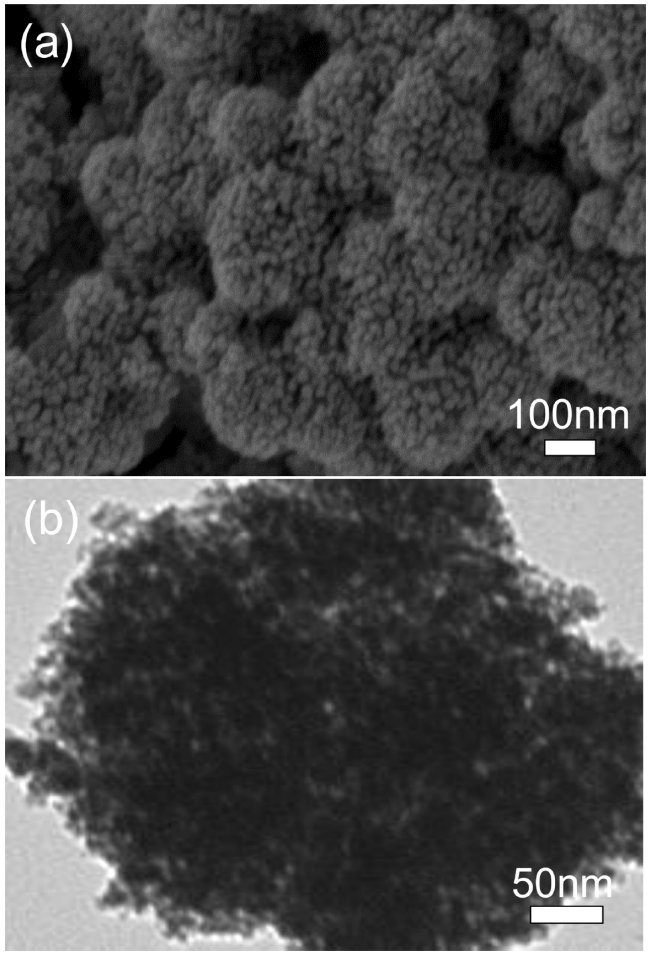

Figure 2. (a) SEM image and (b) TEM image of $MgTiO_3$ perovskite synthesized using the PVC-g-POEM graft copolymer as a template at 150 °C for 10 h.

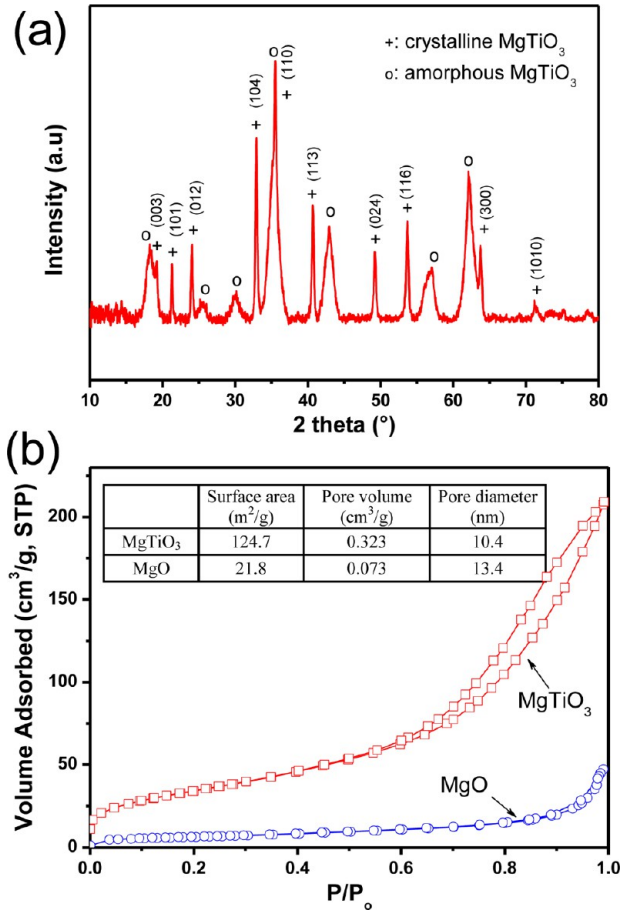

Figure 3. (a) XRD pattern and (b) N_2 adsorption−desorption curve of $MgTiO_3$ perovskite synthesized using the PVC-g-POEM graft copolymer as a template at 150 °C for 10 h. N_2 adsorption−desorption curve of MgO synthesized in the same manner was also included.

dx.doi.org/10.1021/am401306p | ACS Appl. Mater. Interfaces 2013, 5, 6615−6621

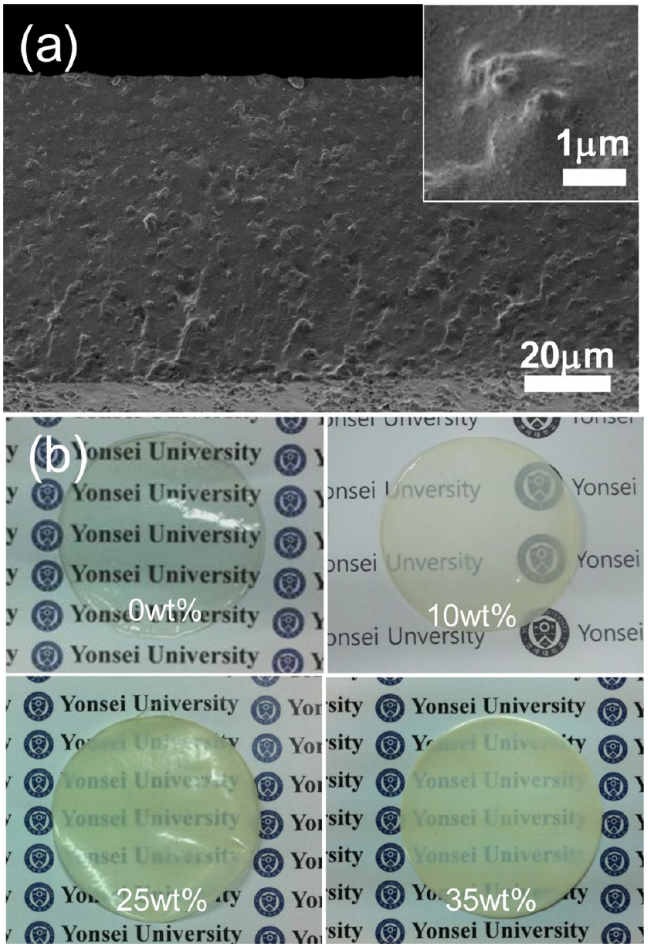

Figure 4. (a) Cross-sectional SEM images of an MMM consisting of PVC-g-POEM and mesoporous $MgTiO_3$ perovskite at a $MgTiO_3$ loading of 35 wt % (inset, magnified image), (b) photos of the MMMs.

uniform distribution of $MgTiO_3$. This demonstrates that the PVC-g-POEM template functioned as a robust and precise structure-directing agent. However, a non-uniform distribution with asymmetric structure was obtained for the MMM containing mesoporous MgO due to a lower porosity (0.22) as shown in Figure S3 in the Supporting Information, indicating the importance of porosity in MMMs. The high magnification cross-sectional SEM image (inset of Figure 4a) also clearly shows good interfacial contact between the inorganic $MgTiO_3$ nanocrystals and organic PVC-g-POEM polymer without any voids or cracks. The PVC-g-POEM graft copolymer functions well as a compatibilizer at the microscopic level due to the flexible, sticky properties of the amorphous, rubbery POEM side chains, preventing void formation at the interface. The transparent PVC-g-POEM graft copolymer membrane becomes translucent with increasing $MgTiO_3$ content, as shown in Figure 4b. Also, the hydrophobic, glassy PVC main chains microphase-separated from the POEM side chains provide good dimensional stability and thus, all of the membranes were mechanically strong with thicknesses of 60−70 μm. The general behavior observed in strain vs. tensile stress curves is that the elongation at break of MMM is reduced with $MgTiO_3$ content (Figure 5). The tensile strength and Young's modulus of MMM were ranged in 8−9 MPa and 8−26 MPa, respectively, indicating good mechanical strength. The good mechanical properties of MMM are attributed to good

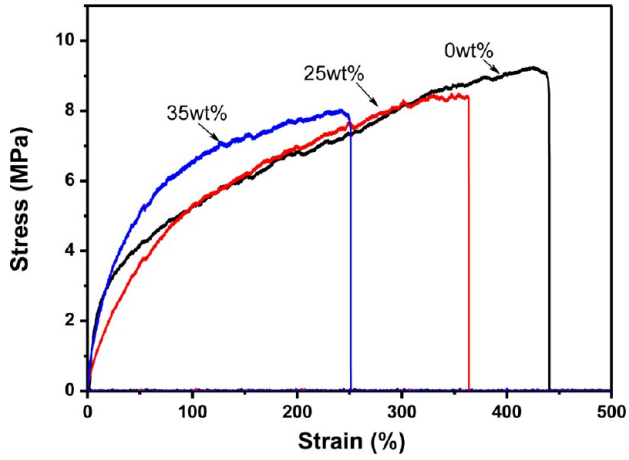

Figure 5. Strain vs. tensile stress curves of MMMs with different amounts of $MgTiO_3$.

interfacial interactions/adhesions at the polymer/$MgTiO_3$ interfaces.

Performance testing was performed for CO_2/N_2 separation, which presents one of the greatest opportunities for CO_2 membrane systems because of the greenhouse gas nature of CO_2. The pure gas permeation properties and CO_2/N_2 ideal selectivity of the MMM were measured using a constant volume/variable pressure apparatus at 760 mmHg and 35 °C (Figure 6a, Table 1). The CO_2 and N_2 permeabilities of a pure PVC homopolymer membrane are as low as 1.7 and 0.06 Barrer (1 Barrer = 1×10^{-10} cm^3(STP) cm cm^{-2} s^{-1} $cmHg^{-1}$), respectively, due to the high chain compactness and low segmental motion of the polymeric chains. Compared to a PVC membrane, both the CO_2 permeability and CO_2/N_2 selectivity through the PVC-g-POEM graft copolymer membrane increased. These improvements arise from the amorphous, rubbery properties of POEM and the high affinity of polar ether oxygens for CO_2.[24] The CO_2 permeability through the PVC-g-POEM/$MgTiO_3$ membranes increased by 140% up to 138.7 Barrer at a $MgTiO_3$ content of 25 wt % without a large loss of CO_2/N_2 selectivity. Mesoporous MgO, which is known to have a high affinity for acidic CO_2 because of its strong basicity,[22,23] was also synthesized in the same manner, as shown in Figure S4 in the Supporting Information. The total pore volume of MgO determined by N_2 adsorption−desorption measurements was 0.073 cm^3/g, which is approximately five-fold smaller than that of $MgTiO_3$ (0.323 cm^3/g). CO_2 temperature-programmed desorption (TPD) measurements[37,38] show that the $MgTiO_3$ perovskite had a basic site density of 0.519 mmol/g, which is approximately 3.4 times higher than MgO (0.153 mmol/g), as shown in Figure 6b. It is due to larger total pore volume and greater surface area of the $MgTiO_3$ perovskite. The CO_2 permeability of PVC-g-POEM/MgO was much smaller than that of the PVC-g-POEM/$MgTiO_3$ membrane with a loading of 10 wt %, indicating the importance of porosity in MMMs. Furthermore, mesoporous TiO_2 (non-interacting with CO_2) with porosity and pore size similar to $MgTiO_3$ perovskite was also synthesized and used to prepare MMM. Despite similar N_2 permeability, the CO_2 permeability of MMM with TiO_2 10 wt % was lower than that with $MgTiO_3$ 10 wt %, indicating the higher CO_2 solubility of $MgTiO_3$. Thus, the improved gas permeability of MMM with $MgTiO_3$ perovskite is due to the simultaneous improvement of solubility and diffusivity. The performances of neat PVC-g-POEM and all the MMMs crosses

dx.doi.org/10.1021/am401306p | ACS Appl. Mater. Interfaces 2013, 5, 6615−6621

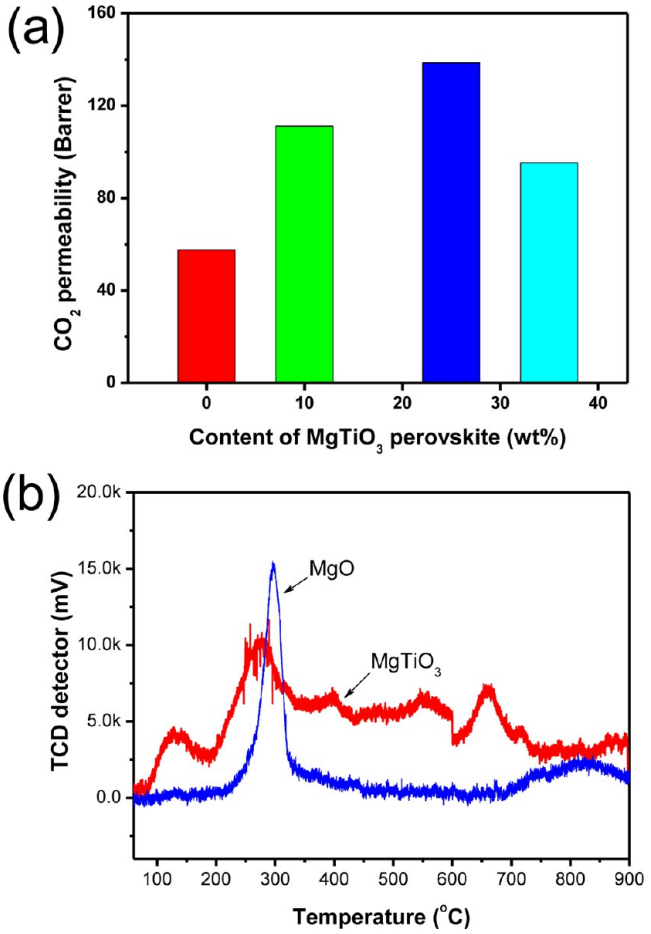

Figure 6. (a) CO_2 permeability of the MMMs measured at 760 Torr and 35 °C, and (b) TPD curves of $MgTiO_3$ and MgO synthesized using the PVC-g-POEM graft copolymer.

Table 1. Pure Gas Permeabilities (P) and CO_2/N_2 Selectivities (α) of Pristine PVC, PVC-g-POEM, and MMMs with Different Amounts (wt %) of $MgTiO_3$, TiO_2, and MgO at 760 mmHg and 35 °C[a]

membrane	P(CO_2) (Barrer)	P(N_2) (Barrer)	α(CO_2/N_2)
PVC	1.7	0.06	28.3
PVC-g-POEM	57.6	1.4	42.3
PVC-g-POEM/$MgTiO_3$ 10%	111.1	2.7	40.5
PVC-g-POEM/$MgTiO_3$ 25%	138.7	3.6	38.2
PVC-g-POEM/$MgTiO_3$ 35%	95.3	2.4	40.0
PVC-g-POEM/TiO_2 10%	90.2	2.6	34.7
PVC-g-POEM/MgO 10%	76.7	2.0	38.9

[a]1 Barrer = 1×10^{-10} cm^3(STP) cm cm^{-2} s^{-1} $cmHg^{-1}$.

the upper bound limit (1991) but lies below the upper bound (2008),[4] as shown in Figure S5 in the Supporting Information. The membrane performances can be improved further by utilizing a more permselective polymer matrix or mesoporous perovskite with a greater basicity. However, it should be also noted that a rubbery, flexible poly(dimethyl siloxane) (PDMS) or cross-linked PEO membrane with a high gas permeability was not able to form mechanically strong MMM because the polymer chains could not undergo cross-linking in the presence of mesoporous $MgTiO_3$ perovskite (PVC-g-POEM graft copolymer does not undergo cross-linking).

CONCLUSION

An approach to design a new class of MMMs for CO_2 separation based on enhancing their diffusivity as well as solubility selectivity was demonstrated using a mesoporous $MgTiO_3$ perovskite. The perovskite with a high porosity and mesopores was synthesized through a solvothermal reaction at 150°C by templating a PVC-g-POEM graft copolymer. Good interfacial properties and uniform distribution in the MMM were obtained due to the high mesoporosity of perovskite and amphiphilic properties of PVC-g-POEM. The CO_2 permeability through the PVC-g-POEM/$MgTiO_3$ membranes increased by 140% up to 138.7 Barrer without a large loss of CO_2/N_2 selectivity. This strategy provides direction for the design of MMM materials for economical CO_2 capture processes.

ASSOCIATED CONTENT

Supporting Information

SEM-EDS, SEM images, and CO_2 permeability vs. CO_2/N_2 selectivity. This material is available free of charge via the Internet at http://pubs.acs.org/.

AUTHOR INFORMATION

Corresponding Author

*E-mail: jonghak@yonsei.ac.kr. Tel: +82-2-2123-5757. Fax: +82-2-312-6401.

Notes

The authors declare no competing financial interest.

ACKNOWLEDGMENTS

We acknowledge financial support from National Research Foundation (NRF) grant funded by the Korean government (MEST) through the Korea CCS R&D Center, the Korea Center for Artificial Photosynthesis (KCAP) (2012M1A2A2671781), the Core Research Program (2012R1A2A2A02011268), and the Energy Efficiency & Resources of the Korea Institute of Energy Technology Evaluation and Planning (KETEP) grant (20122010100040).

REFERENCES

(1) Snaith, H. J.; Schmidt-Mende, L. *Adv. Mater.* **2007**, *19*, 3187−3200.
(2) Wang, J.; Zhou, Y.; Hu, Y.; O'Hayre, R.; Shao, Z. *J. Phys. Chem. C* **2011**, *115*, 2529−2536.
(3) Lu, J.; Lu, S.; Jiang, S. P. *Chem. Commun.* **2011**, *47*, 3216−3218.
(4) Robeson, L. M. *J. Membr. Sci.* **2008**, *320*, 390−400.
(5) Du, N.; Park, H. B.; Robertson, G. P.; Dal-Cin, M. M.; Visser, T.; Scoles, L.; Guiver, M. D. *Nat. Mater.* **2011**, *10*, 372−375.
(6) Bernardo, P.; Drioli, E.; Golemme, G. *Ind. Eng. Chem. Res.* **2009**, *48*, 4638−4663.
(7) Park, H. B.; Jung, C. H.; Lee, Y. M.; Hill, A. J.; Pas, S. J.; Mudie, S. T.; Wagner, E. V.; Freeman, B. D.; Cookson, D. J. *Science* **2007**, *318*, 254−258.
(8) Du, N.; Park, H. B.; Dal-Cin, M. M.; Guiver, M. D. *Energy Environ. Sci.* **2012**, *5*, 7306−7322.
(9) Xiao, Y.; Chung, T. -S. *Energy Environ. Sci.* **2011**, *4*, 201−208.
(10) Montagne, F.; Blondiaux, N.; Bojko, A.; Pugin, R. *Nanoscale* **2012**, *4*, 5880−5886.
(11) Schrier, J. *ACS Appl. Mater. Interfaces* **2013**, *4*, 3745−3752.
(12) Car, A.; Stropnik, C.; Yave, W.; Peinemann, K. -V. *J. Membr. Sci.* **2008**, *307*, 88−95.

(13) Lin, H.; Wagner, E. V.; Raharjo, R.; Freeman, B. D.; Roman, I. *Adv. Mater.* **2006**, *18*, 39−44.
(14) Lin, H.; Wagner, E.V.; Freeman, B. D.; Toy, L. G.; Gupta, R.P. *Science* **2006**, *311*, 639−642.
(15) Car, A.; Stropnik, C.; Yave, W.; Peinemann, K.-V. *Adv. Func. Mater.* **2008**, *18*, 2815−2823.
(16) Simons, K.; Nijmeijer, K.; Bara, J. E.; Noble, R. D.; Wessling, M. *J. Membr. Sci.* **2010**, *360*, 202−209.
(17) Bara, J. E.; Carlisle, T. K.; Gabriel, C. J.; Camper, D.; Finotello, A.; Gin, D. L.; Noble., R. D. *Ind. Eng. Chem. Res.* **2009**, *48*, 2739−2751.
(18) Gu, Y.; Lodge, T. P. *Macromolecules* **2011**, *44*, 1732−1736.
(19) Chung, T. -S.; Jiang, L. Y.; Li, Y.; Kulprathipanja, S. *Prog. Polym. Sci.* **2007**, *32*, 483−507.
(20) Patel, N. P.; Miller, A. C.; Spontak, R. J. *Adv. Mater.* **2003**, *15*, 729−733.
(21) Patel, N. P.; Miller, A. C.; Spontak, R. J. *Adv. Funct. Mater.* **2004**, *14*, 699−707.
(22) Matteucci, S.; Kusuma, V. A.; Kelman, S. D.; Freeman, B. D. *Polymer* **2008**, *49*, 1659−1675.
(23) Buonomenna, M.G.; Yave, W.; Golemme, G. *RSC Adv.* **2012**, *2*, 10745−10773.
(24) Ahn, S. H.; Seo, J. A.; Kim, J. H.; Ko, Y.; Hong, S. U. *J. Membr. Sci.* **2009**, *345*, 128−133.
(25) Ahn, S. H.; Chi, W. S.; Park, J. T.; Koh, J. K.; Roh, D. K.; Kim, J. H. *Adv. Mater.* **2012**, *24*, 519−522.
(26) Park, J. T.; Prosser, J. H.; Ahn, S. H.; Kim, S. J.; Kim, J. H.; Lee, D. *Adv. Funct. Mater.* **2013**, *23*, 2193−2200.
(27) Feng, C.; Li, Y.; Yang, D.; Hu, J.; Zhang, X.; Huang, X. *Chem. Soc. Rev.* **2011**, *40*, 1282−1295.
(28) Zhang, M.; Russell, T. P. *Macromolecules* **2006**, *39*, 3531−3539.
(29) Kim, Y. W.; Choi, J. K.; Park, J. T.; Kim, J. H. *J. Membr. Sci.* **2008**, *313*, 315−322.
(30) Bicerano, J. *Prediction of Polymer Properties*, 2nd ed.; Marcel Dekker: New York, 1996.
(31) Ahn, S. H.; Park, J. T.; Koh, J. K.; Roh, D. K.; Kim, J. H. *Chem. Commun.* **2011**, *47*, 5882−5884.
(32) Zhou, X.; Yuan, Y.; Xiang, L.; Huang, Y. *J. Mater. Sci.* **2007**, *42*, 6628−6632.
(33) Ferri, E. A.V.; Sczancoskia, J. C.; Cavalcantea, L. S.; Paris, E. C.; Espinosa, J. W. M.; de Figueiredo, A. T.; Pizania, P. S.; Mastelaro, V. R.; Varela, J. A.; Longo, E. *Mater. Chem. Phys.* **2009**, *117*, 192−198.
(34) Zhou, X.; Yuan, Y.; Xiang, L.; Huang, Y. *J. Mater. Sci.* **2007**, *42*, 6628−6632.
(35) Vandermiers, C.; Damman, P.; Dosière, M. *Polymer* **1998**, *39*, 5627−5631.
(36) Nakade, S.; Kanzake, T.; Wada, Y.; Yanagida, S. *Langmuir* **2005**, *21*, 10803−10807.
(37) Serio, M. D.; Ledda, M.; Cozzolino, M.; Minutillo, G.; Tesser, R.; Santacesaria, E. *Ind. Eng. Chem. Res.* **2006**, *45*, 3009−3014.
(38) Li, E.; Rudolph, V. *Energy Fuels* **2008**, *22*, 145−149.